

promoting access to White Rose research papers



Universities of Leeds, Sheffield and York
<http://eprints.whiterose.ac.uk/>

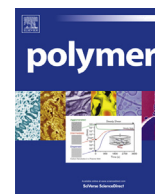
This is a copy of the final published version of a paper published via gold open access in **Polymer**

This open access article is distributed under the terms of the Creative Commons Attribution Licence (<http://creativecommons.org/licenses/by/3.0>), which permits unrestricted use, distribution, and reproduction in any medium, provided the original work is properly cited.

White Rose Research Online URL for this paper:
<http://eprints.whiterose.ac.uk/88540>

Published paper

Laity, P.R., Gilks, S.E. and Holland, C. (2015) *Rheological behaviour of native silk feedstocks*. *Polymer*, 67. 28 - 39
10.1016/j.polymer.2015.04.049



Rheological behaviour of native silk feedstocks



P.R. Laity^{a,*}, S.E. Gilks^{a,b}, C. Holland^a

^a Department of Materials Science and Engineering, The University of Sheffield, Sir Robert Hadfield Building, Mappin Street, Sheffield, S1 3JD, UK

^b School of Chemical Engineering and Analytical Science (CEAS), The Mill, The University of Manchester, Oxford Road, Manchester, M13 9PL, UK

ARTICLE INFO

Article history:

Received 28 January 2015

Received in revised form

8 April 2015

Accepted 16 April 2015

Available online 28 April 2015

Keywords:

Native Silk

Rheology

Bombyx mori

ABSTRACT

Whilst much is known about the properties of silks, the means by which native silk feedstocks are spun still represent a gap in our knowledge. Rheology of the native silk feedstocks is germane to an understanding of the natural spinning process. Yet, an overview of the literature reveals subtle limitations and inconsistencies between studies, which has been largely attributed to sample-to-sample variation when testing these exquisitely flow-sensitive materials. This ambiguity has prevented reliable, consistent inferences from standard polymer rheology and constitutes an obstacle to further development.

To address this challenge, we present the largest study to date into the rheological properties of native silk feedstocks from *Bombyx mori* larvae. A combination of shear and oscillatory measurements were used to examine in detail the relationships between concentration, low shear viscosity, relaxation times, complex modulus and estimates of the molecular weights between entanglements. The results from this highly detailed survey will provide a sound basis for further experimental or theoretical work and lay the foundations for future bio-inspired processing of proteins.

© 2015 The Authors. Published by Elsevier Ltd. This is an open access article under the CC BY license (<http://creativecommons.org/licenses/by/4.0/>).

1. Introduction

Silks are natural protein fibres spun by many types of arthropods in the classes Arachnida, Insecta and Myriapoda [1–11]. This may be a significant example of convergent evolution, as the ability to produce silk appears to have arisen independently at least 23 times [8]. Spiders provide the most widespread and obvious examples of silk production, with some recently evolved spider species producing at least seven different types throughout their entire lifecycle, as distinguished by chemical compositions, gland morphologies, physical properties and the ways the fibres are used by the animal [1–4]. The larvae of various lepidoptera (*i.e.* caterpillars) appear to produce only one type of silk at any time, although the quantities and compositions vary between species [5] and developmental stage [12]. Most notably, as a result of millennia of selective human intervention, the domesticated mulberry silkworm *Bombyx mori*, produces relatively large quantities of cocoon silk, which has achieved considerable importance as a textile fibre [13–16].

Although the amino-acid sequences vary, the main proteins in lepidoptera and spider silks (*i.e.* fibroins and spidroins) appear to

follow a common theme. A large (up to 500 kDa) highly repetitive core section accounts for the high degree of order and partial crystallinity that can be observed in silk fibres [16–25]. The core is flanked by short non-repetitive globular terminal domains (typically 10–15 kDa), which appear to promote association with other chains in solution, through physical interactions initiated by a decrease in pH and changes in ion content [26–31].

Typically, several different proteins are present in a single type of silk fibre. In *B. mori* silk the main fibroin component consists of a ‘heavy’ (fibH) chain, with molecular weight around 350–400 kDa [32–35]. This is joined by a disulphide bond near its C-terminus to a ‘light’ (fibL) chain with molecular weight around 25–30 kDa [34–38]. This fibH-fibL dimer appears to be important for efficient secretion of fibroin and maintaining good solubility within the silk gland, as ‘naked pupa’ mutants lacking genes for fibL chain expression produce only small amounts of exclusively fibH silk [39–41]. The fibH-fibL dimer forms non-covalent interactions with a ‘P25’ chaperone (*ca.* 27–30 kDa) glycoprotein [42–45], to give a (fibH-fibL)₆P25₁ complex of molecular weight around 2.3 MDa [46]. There is evidence that complexes of this type may be common, though not universal in lepidopteran silks [47] and may facilitate intracellular transport [46], although any subsequent role in silk spinning remains unknown.

In addition to the major fibroin components of lepidopteran silks, many minor components have been observed. Analyses of

* Corresponding author. Tel.: +44 114 222 6018.

E-mail address: petelaity@aol.com (P.R. Laity).

materials from *B. mori* silk glands revealed several components of sericin, which forms an adhesive sheath around the fibrous fibroin core, and over 500 minor species with molecular weights ranging from 15 to 100 kDa [12,34,38,48]. These appeared to include chaperones, heat-shock proteins, protease inhibitors and other metabolic enzymes, although their contributions to the spinning process also remain unknown.

Hence, given the considerable structural, compositional and functional diversities shown by silks, their means of production (*i.e.* spinning) may provide a more appropriate definition, as suggested by Porter and Vollrath [49]. It is a characteristic of all silks that they are initially produced as hydrated protein feedstocks (typically 20–30 % w/w), stored within the animal in specialised glands then, when required, extruded relatively quickly into fibres [1,2,5,8,18,49–51]. Typically, silkworms produce fibre for cocoon construction at 4–15 mm s⁻¹ and spiders can produce major ampullate (*i.e.* dragline) silks at 20–60 mm s⁻¹ [52,53], while take-up speeds of 400 mm s⁻¹ have been achieved during forced reeling [54]. This ‘on demand’ nature of silk spinning is in stark contrast to other fibres produced by animals (*i.e.* hair or wool), which grow continuously at relatively slow speeds; for example, Downes and Sharry [55] reported a growth rate of around 0.3–0.4 mm per day for sheep wool. The importance of the spinning process on silk fibre mechanical properties has been well documented and is considered to be as crucial as the feedstock itself [21,52,54,56–61].

While much has been written concerning the remarkable properties and uses of silk fibres [16,19,21,49–53,62], we suggest that the natural spinning route represents the most inspirational feature of silks. During silk spinning, the animal is able to convert a high molecular weight polymer from an aqueous (solution or gel) phase into a water-insoluble fibre, rapidly and at ambient temperatures [3,18,19,48,52,53,55,63,64]. This transition to a solid silk fibre appears to be initiated by flow-induced alignment of the protein chains [54,65,66], probably after the system has been activated by changes in pH and ionic content within the silk duct [26–31,66–69]. The only significant energy input for this process would appear to be the work required to convey the protein feedstock along the silk duct and draw it into a fibre.

By comparison, melt-spun fibres of thermoplastic polymers (*e.g.* polyolefins or polyesters) are typically extruded around 200–300 °C above ambient temperature, while wet- or dry-spun fibres (*e.g.* viscose rayon, acrylics or cellulose acetate) involve large amounts of harmful and potentially dangerous solvents or other processing chemicals [70,71]. Each of these processing routes incurs a significant energy penalty (*e.g.* for process heating or solvent recovery, where applicable) and may also produce pollution in the form of spent or unrecoverable process chemicals. This disparity in energy efficiency between natural silks and synthetic polymers has been recently highlighted by Holland *et al.* [64], who estimated that the energy required to initiate the phase-change in silk would be several orders of magnitude smaller than that required to melt-spin high density polyethylene.

Rheology provides a convenient and informative method for characterising the behaviour of polymer-based and colloidal systems [72–76]. Meaningful measurements can be made on a wide range of flowable media (including solutions, suspensions, melts, gels, pastes and granular systems) under realistic conditions, using modest quantities of materials (*i.e.* consistent with the volumes of silk feedstock contained in the ducts of *B. mori*, other silkworms and reasonably large spiders). Moreover, in polymer-based systems, a suitable analysis of oscillatory measurements can yield information on chain entanglements, relaxation rates and molecular weight. In view of the role generally ascribed to interchain interactions, flow-induced orientation and phase transformations, information of this type is considered to be germane for a complete understanding of

natural silk spinning. Consequently, a large body of work has already been published concerning rheological properties of native silk feedstock from *B. mori* [65,66,77–85], other silkworms [82,83], spiders [84,86,87], as well as reconstituted silk feedstocks prepared using various chaotropic solvents [85,88–94].

This has revealed some important generic rheological characteristics across all native silk feedstocks tested to date. Specimens undergo shear-thinning (*i.e.* the viscosity decreases as shear rate increases) [65,78–87] accompanied by flow-induced orientation [65,66,81]. They also exhibit significant viscoelasticity, with the elastic or storage modulus (G') exceeding the viscous or loss modulus (G'') at high frequency and a cross-over to viscous behaviour ($G' < G''$) at low frequency [65,78,80–85]. These observations are typical of a concentrated polymer solution above the overlap threshold, where the rheology is dominated by interchain entanglements [72–76]. Moreover, comparisons between specimens from *B. mori* and wild types suggest that silkworms can produce superficially similar fibres from protein solutions with somewhat different rheological characteristics [82,83].

Nevertheless, a careful examination of the details reveals several limitations and inconsistencies amongst this work. For example, for native silk feedstocks from *B. mori*, the reported values of low shear-rate (*i.e.* $\dot{\gamma} < 0.1 \text{ s}^{-1}$) viscosity range from 10³ to 10⁸ Pa s [65,66,77–85]. Also, the cross-over from elastic to viscous behaviour (at $G' = G''$) has been reported at angular frequencies ranging from 1 to 10 rad s⁻¹ [65,78,80–85]. By contrast, the data presented by Ochi *et al.* [77] was more characteristic of a gel, with $G' > G''$ over the entire frequency range. It is possible that these apparent inconsistencies may reflect inherent variations in a natural biological system, or they may have resulted from poor handling of a highly sensitive material. This ambiguity has prevented reliable, consistent inferences based on standard polymer rheological analysis and constitutes a considerable obstacle to further development of the field. We propose that this may be addressed by adopting a more statistical approach to the analysis of native silk rheology and studying the distributions of properties.

The purpose of the present work was to provide a thorough analysis of the rheological characteristics exhibited by native silk protein feedstock from a statistically meaningful population of the silkworm *B. mori* at 25 °C. To that effect, combinations of shear and oscillatory measurements were used to extract information on molecular relaxation behaviour and chain entanglements. This will provide the background for subsequent work on silk protein solutions, including measurements of the activation energy of flow, investigating shear- and temperature-induced gelation, comparisons between native feedstocks from other animals and the characterisation of redissolved silk protein systems.

2. Experimental

B. mori silkworms in the 5th instar were housed at ambient humidity until ready for use. Once the silkworms had stopped feeding, they were housed at around 10 °C, in order to delay pupation (normally by no more than 10 days). In addition to visual examination, the weights of some silkworms were monitored in order to assess their condition during storage.

Native silk feedstocks were extracted from silkworms that had just started to construct the cocoon. The silk glands were removed following methods similar to those described previously [65,82,85]. Using a dissection microscope, glands were carefully separated from the rest of the tissue, then transferred to cold (*ca.* 5 °C) distilled water in order to peel off the epithelial membrane using tweezers. This was achieved as quickly as possible (typically within 5 min) to minimise dilution of the silk gland contents. The coiled

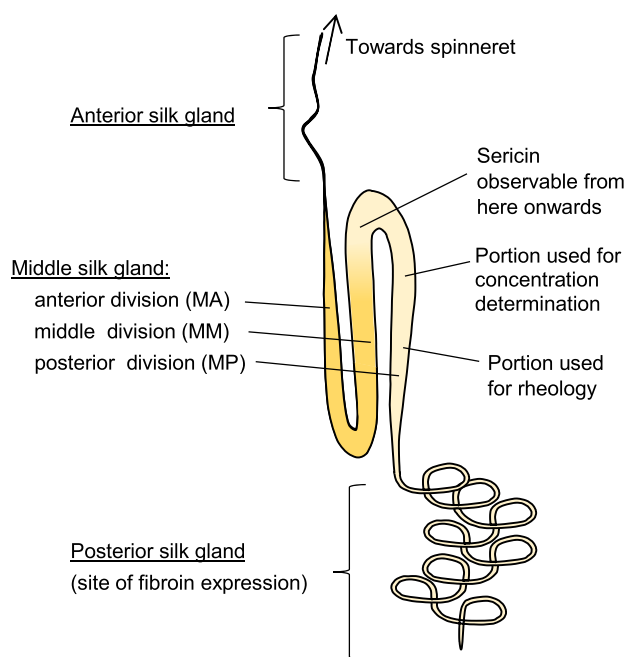


Fig. 1. Diagram of *B. mori* silk gland, showing portions used for measurements.

posterior gland and thin anterior duct (shown diagrammatically in Fig. 1) were separated off and discarded.

Close examination of the middle gland under the microscope revealed the presence of two concentric phases in the middle and anterior (MM and MA) divisions. The central region was believed to be fibroin solution, which was produced in the posterior gland, while the outer was ascribed to the addition of sericin in the middle gland [34,46,48]. Hence, to optimise the extraction of fibroin solution, while minimising the inclusion of sericin, only the single-phase contents obtained from the hindmost section of the middle division (MP) of the silk gland was used for rheological measurements. It may be noted that a similar approach was also used previously by Boulet-Audet *et al.* [81].

Small portions of gland contents (*ca.* 0.01–0.02 g) were carefully collected between the tips of tweezers; excess surface water was removed by dabbing against tissue paper, before gently placing the specimen onto the rheometer plate. Excessive handling stresses were avoided throughout this procedure, to minimise the risk of shear-induced gelation [65,84]. At the same time, a larger sample (*ca.* 0.08–0.1 g) was also collected from the adjacent part of the silk gland, which was used to measure the solids content (*c*) gravimetrically, after drying to constant weight under vacuum at 60 °C.

2.1. Spectroscopic characterisation

Fourier-transform infrared spectroscopy (FTIR) was performed using a Nicolet 380 spectrometer (Thermo Scientific, Madison, USA) fitted with an attenuated total reflection (ATR) device (Golden Gate, 45° single-bounce diamond anvil, Specac, UK). The optical path through the spectrometer and ATR device was purged using dry air from which CO₂ had been removed, in order to minimise background absorbance. Liquid specimens of gland contents were simply placed on the ATR device and covered with a microscope cover slip to prevent water evaporation. Solid residue was first cast into a thin film by diluting the gland contents in distilled water (approx. 20 × with gentle swirling), pouring the diluted solution into a plastic weighing boat and allowing the water to evaporate in a stream of flowing air; the film was subsequently peeled off the

weighing boat and clamped to the ATR device. Spectral data between 800 and 4000 cm⁻¹ was obtained by collecting 32 scans at 4 cm⁻¹ resolution. Corrections for background absorbance and sampling depth of the ATR method were applied.

2.2. Rheology

Rheological measurements were performed using a Bohlin Gemini (Malvern Instruments, UK) rheometer, incorporating a Peltier (heating and cooling) stage, with a CP1/10 cone and plate geometry (5.00 mm radius, 1° opening angle and 30 μm truncation). Silk protein solution, sufficient to completely fill the geometry, was placed on the plate (fixed) and the cone (driven) was lowered to the required gap setting (30 μm); the closing speed was reduced to the minimum (*ca.* 0.1 mm s⁻¹) before the cone touched the fibroin solution. Excess solution was allowed to squeeze out from under the cone and was not removed, to avoid shear induced gelation at the edge of the geometry. To avoid the specimen drying out and forming a skin, the area outside the cone was flooded with distilled water and loosely enclosed using an environmental chamber, which was designed to fit around the cone and drive shaft without touching.

The majority of experiments were performed in two stages. First, a constant shear rate of $\dot{\gamma} = 1 \text{ s}^{-1}$ was applied for 100 s at 25 °C, in order to ensure the specimen was distributed evenly between the cone and plate and to establish a uniform rheological state (*i.e.* superseding any residual stress from sample loading). The shear viscosity at $\dot{\gamma} = 1 \text{ s}^{-1}$ (η_1) was obtained by averaging data from the final 30 s of this stage. Then, a series of oscillatory measurements of elastic (*i.e.* storage) and viscous (*i.e.* loss) moduli (G' and G'') were performed from 25 to 0.1 Hz (equivalent to 157 to 0.63 rad s⁻¹), using an applied strain of 0.02, which is within the linear viscoelastic limit of the silk protein solution (see supplementary information given by Holland *et al.* [84]).

In order to investigate certain experimental observations in greater detail, a few experiments were also performed incorporating modified or repeated stages, as described in the text below.

3. Results

In order to confirm the composition of the silk protein feedstocks used, FTIR spectra of the native silk protein solution and dried films are presented in Fig. 2, along with assignments of the main bands. The solution spectrum was dominated by the strong O–H stretching (3000–3700 cm⁻¹) and weaker bending (1630 cm⁻¹) bands of water, which was the largest component. Only the relatively strong amide II (1520 cm⁻¹) and amide III (1230 cm⁻¹) bands of the protein could be observed clearly. By comparison, a large number of peaks associated with protein were evident in the spectra of the dried films. These included the amide I, II and III bands (at 1633, 1512 and 1230 cm⁻¹), the broad absorbance (between 3200 and 3600 cm⁻¹) due to multiple O–H and N–H stretching vibrations and the small peaks ascribed to aliphatic C–H stretching (around 2900 cm⁻¹). The small peak at 3062 cm⁻¹ may be ascribed to the aromatic C–H stretching band of tyrosine [95], which constitutes around 5% (molar) of the amino acids in *B. mori* silk proteins [16,34,35]. The peaks around 983, 1050 and 1400 cm⁻¹ may be ascribed to C–O stretching and C–O–H bending vibrations of serine [96,97], which constitutes around 12% (molar) of the amino acids in *B. mori* fibroin or 30% in sericin [16,34,35]. At least another 10 small, unassigned peaks were also evident between 900 and 1500 cm⁻¹.

Comparison between films prepared using solutions from the MP and MM sections of the gland revealed slightly larger peaks ascribed to serine (*ca.* 983, 1050 and 1400 cm⁻¹) in the latter. These

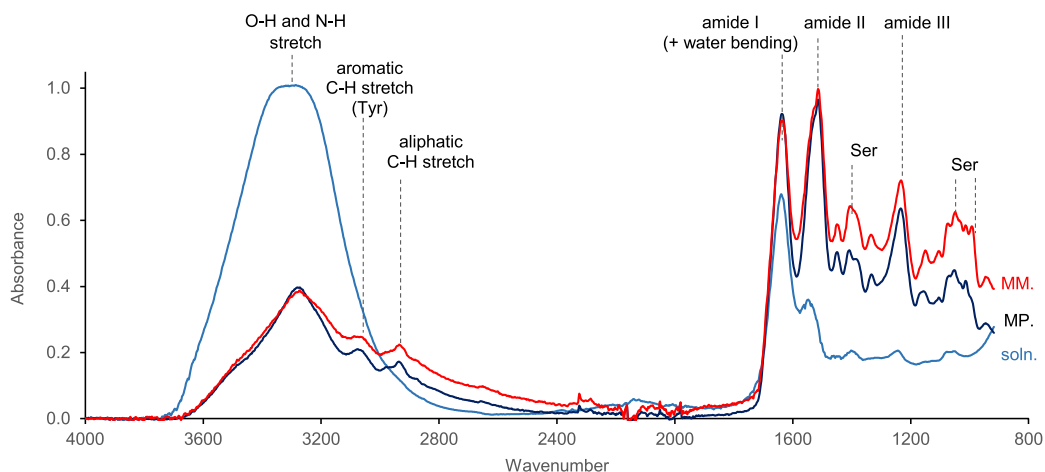


Fig. 2. FTIR spectra of native silk protein solution (soln.) and dried films (at ambient moisture), prepared using solution samples collected from the middle (MM) and posterior (MP) divisions of the middle gland. Peaks attributable to serine are marked (Ser).

differences suggested a higher proportion of sericin in the MM section, compared with the MP section, which agreed qualitatively with results from gel electrophoresis reported by Gamo *et al.* [34]. In conjunction with reports of the relatively small amounts of inorganic salts present in the native silk solution [98], these results suggested that fibroin was the main solid component of the specimens used for rheology, although it is likely that minor amounts of sericin may have also been present.

3.1. Gland contents concentration

The solids contents measured in samples of native silk protein solutions are presented in Fig. 3. Due to the limited quantity of material available (generally less than 0.1 g of native solution, containing less than 0.02 g of solids), the uncertainty due to weighing errors was typically $\pm 1\%$ w/w. Nevertheless, considerable variations in concentration were observed, which exceeded this uncertainty.

Based on the analysis of 124 samples, the solids contents ranged from 18.7 to 30.0 % w/w, with a mode around 24% w/w, as shown in Fig. 3a. The results appeared to approximately follow a normal distribution with a mean of 24.0% and standard deviation of 2.5% w/w. This range also encompassed the compositions reported previously [65,66,77–85].

It was found that the silkworms lost around 3% of body mass per day, during storage at ambient humidity and 10 °C. Nevertheless, there appeared to be negligible change in the solids contents of the native silk feedstocks over 15 days storage under those conditions, as shown in Fig. 3b. It should also be noted that silkworms for rheological experiments were normally not stored for more than 10 days.

These results indicated significant sample-to-sample variations in solids content, in spite of taking only specimens from similar portions of the silk ducts (MP section – see Fig. 1) of silkworms at similar stages of development (5th instar at the start of pupation and up to 10 days storage at 10 °C), using consistent handling procedures.

3.2. Shear viscosity measurements

Plots of apparent viscosity at $\dot{\gamma} = 1 \text{ s}^{-1}$ measured over 100 s are compared in Fig. 4. Apparent shear viscosities were estimated by averaging the final 30 s of each measurement. For the examples shown in Fig. 4, the results ranged from 418 to 3304 Pa s; this range

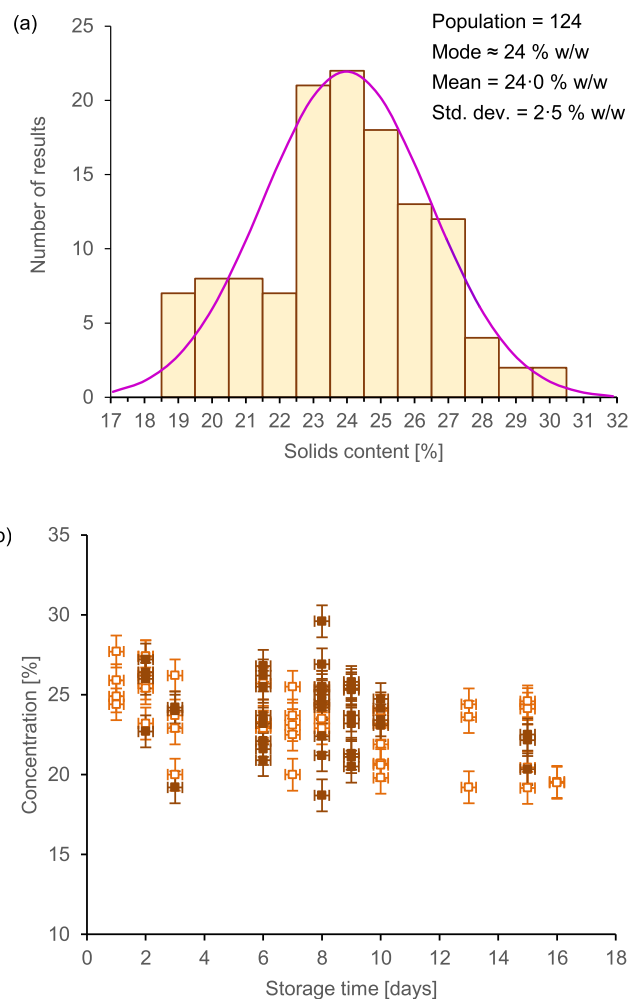


Fig. 3. (a) Histogram showing the distribution of native silk protein concentrations, based on the population size shown; the continuous line represents the normal distribution approximating the results obtained, with the mean and standard deviation shown. (b) Plot of silk concentration against the number of days specimens were stored at 10 °C, for two batches of silkworms (filled and open symbols); the horizontal error bars represent ± 0.25 days, the vertical error bars represent the uncertainty ($\pm 1\%$ w/w) in determining the solids contents of the small (*ca.* 0.1 g) specimens measured.

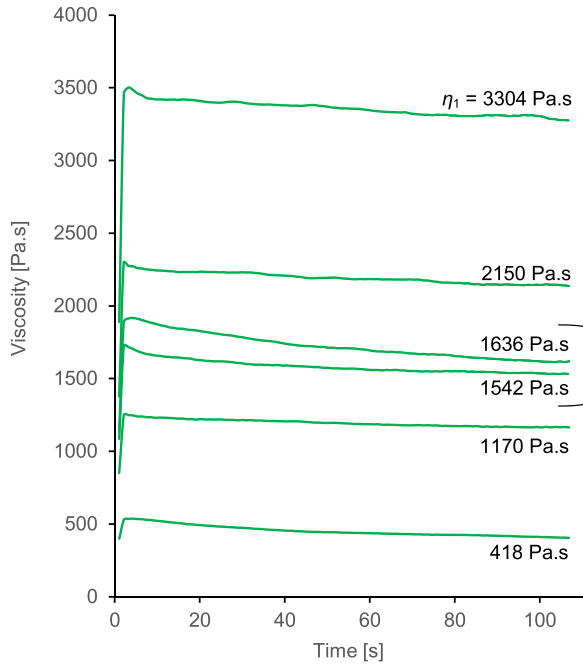


Fig. 4. Variation in (apparent) shear viscosity over 100 s at $\dot{\gamma} = 1 \text{ s}^{-1}$; the values obtained by averaging the final 30 s of data from each specimen are shown; the bracket indicates duplicate measurements on the same specimen.

was considerably greater than the expected uncertainty in the individual measurements and demonstrated the considerable variations in η_1 shown by these silk protein solutions. Further demonstration of this variation is also provided in Fig. 5; based on measurements of 125 specimens, η_1 ranged from 50 to 6018 Pa s. The distribution of values appeared to be skewed, with the mode around 1200 Pa s, the mean at 1722 Pa s, a standard deviation of 935 Pa s and an extended tail towards higher viscosities. There also appeared to be some evidence of bimodality, with clustering around a subsidiary mode at $\eta_1 \approx 1800 \text{ Pa s}$. No obvious

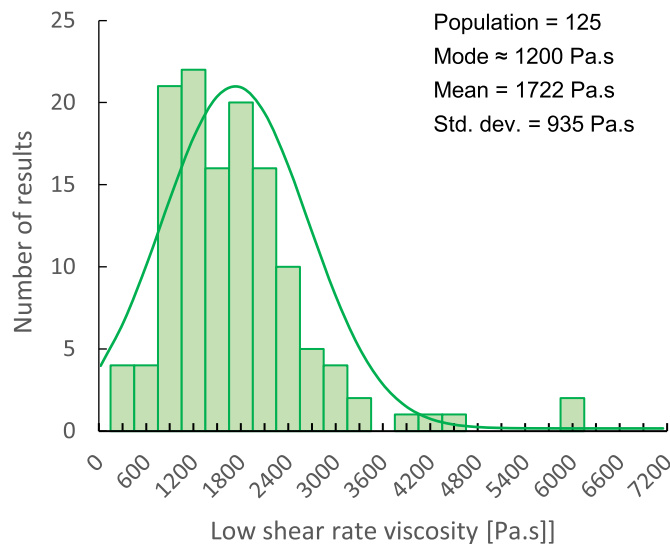


Fig. 5. Histogram showing the distribution of shear viscosity at $\dot{\gamma} = 1 \text{ s}^{-1}$, based on the population size shown; continuous line represents the normal distribution approximating the results obtained, with the mean and standard deviation shown.

correlations could be found between the viscosity, physical condition of the silkworm or storage time.

It is generally expected that the viscosity of a polymer solution increases with concentration, following power-law behaviour in the form of:

$$\eta \propto c^a \quad (1)$$

where a is a constant [72–74]. This was tested for the native silk protein solutions by plotting η_1 against c in Fig. 6, based on the complete set of 124 specimens for which reliable viscosity and concentration data were available. The vertical error bars represent $\pm 100 \text{ Pa s}$, which is expected to be considerably larger than the actual uncertainty in measuring the viscosity; the horizontal error bars ($\pm 1\% \text{ w/w}$) represent the uncertainty in determining the solids content. The continuous curve in Fig. 6 represents the best fit for a power-law relationship, which was achieved with $a = 2.26$. It may be noted that an exponent close to 2 appears to match previously reported results for native *B. mori* silk protein feedstocks [85] and fits with expectations for a polymer solution in the ‘semi-dilute’ concentration range [73]. The correlation coefficient (R^2) was only 0.21, however, suggesting that most of the variation observed in the viscosity was due to factors other than concentration.

Several factors may be invoked to explain the rest of the viscosity variation. Firstly, for polymer solutions above the entanglement threshold concentration, the viscosity is expected to depend strongly on molecular weight [72–76]:

$$\eta \propto M^{3.4} \quad (2)$$

As noted by Craig and Riekel [17], genes encoding for silk proteins are prone to recombination errors due to their length, repetitive nature and codon biases. Manning and Gage [33] observed considerable polymorphism in the silk fibroin genes from different inbred stocks of *B. mori*, which produced a range of fibroin proteins with the molecular weight of the longest (ca. 410 kDa) around 15% higher than the shortest. Although this may be expected to produce

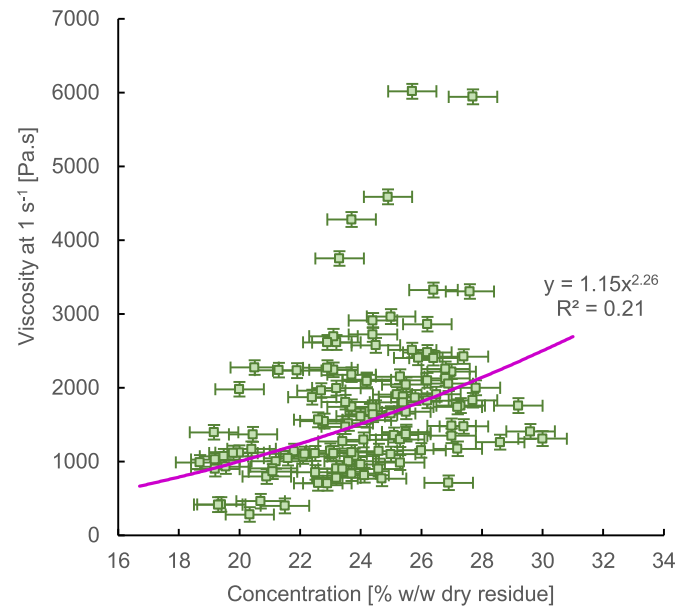


Fig. 6. Plot of shear viscosity at $\dot{\gamma} = 1 \text{ s}^{-1}$ against silk protein concentration (% w/w dry residue); the continuous line represents the best fit power-law relationship. The horizontal error bars represent $\pm 1\% \text{ w/w}$, the vertical error bars ($\pm 100 \text{ Pa s}$) are expected to be considerably larger than the actual uncertainty in viscosity measurements.

significant differences in viscosity, it does not appear sufficient to account for the distribution of observed values, even in combination with the variations in concentration. In view of the expected power-law behaviour described by Equation (2), if the viscosity variation were entirely due to the length of the fibroin protein chains, the observed variations of η_1 would require the highest molecular weight to be around 2.2 times the lowest. This is considerably more than the variation observed by Manning and Gage [33] and thus appears unlikely to provide the complete explanation.

Even if the molecular weights of the fibroin proteins remained constant, a second explanation may involve changes in the relative amounts of species present. Although the fibroin components were expected to constitute the main proteins in the portions of silk gland contents used, a number of other species may have also been present [12,34,37,38,46–48]. Hence, variations in the effective molecular weights of the mixtures could have arisen through changes in their relative proportions.

A third potential explanation may involve differential complexation between the fibH-fibL dimer and the P25 chaperone [44]. The dissolution of protein as free chains or in the (fibH-fibL)₆P25 complex would represent considerable differences in the effective molecular weights of the polymers, which would be expected to produce correspondingly large changes in viscosity.

The viscosity may also be affected by the quality of the solvation and the relative strength of interactions between chain segments. This is usually described by a ‘monomer friction coefficient’ in the various theoretical viscosity models [72–76,99]. Previous work has suggested that interchain interactions may be affected by pH and ion content [26–30,67–69], while Terry *et al.* [65] have already demonstrated the effect of pH on the viscosity of silk protein feedstocks. A full investigation into these (and any other) potential explanations is beyond the scope of the present work, but will be addressed in subsequent studies.

In addition to the obvious differences between specimens, variations in the apparent viscosities were also observed during each measurement. As shown in Fig. 4, each plot appeared to follow a similar trend, rising steeply to a peak within the first few seconds of measurements (as the rheometer responded to the onset of flow), followed by a gradual decline (equivalent to around 10% of the peak value) during the rest of the experiment. This gradual decrease in the apparent viscosity at constant shear rate during the measurement was typical of all the shear data obtained in the present work and has been alluded to previously [65], although no definite explanation could be found in any of the previously reported rheological studies of silk protein feedstocks.

In principle, there may be several possible explanations for this behaviour, involving practical issues of the cone and plate geometry or physical behaviour of the material. These include dilution of the specimen due to the surrounding water, detachment of excess sample from outside the cone circumference, partial ejection of the specimen from between the cone and plate due to normal stress, stress-induced depolymerisation, a yield stress (*i.e.* typical of a Bingham fluid), residual stress from extensional flow during sample loading, non-linear viscoelastic effects and ‘stress overshoot’ as the specimen responded to the onset of shear flow. Clearly, it was important to investigate this behaviour, as it might have affected subsequent measurements. Consequently, the method was modified to include a second steady shear rate measurement (9 experiments) or a series of shear rate jumps (5 experiments) after the initial shear measurement and oscillatory sweep.

Typical results from repeated steady shear measurements are shown (bracketed) in Fig. 4. Although the second run gave a slightly lower viscosity (1542 Pa s) than the first (1636 Pa s), both followed similar shapes. Artefacts due to residual stress from loading

appeared unlikely in the later measurements, which followed the initial shear and oscillatory sweep measurements (*i.e.* at *ca.* 7 min. into the rheology experiment). Also, the second plot started at a higher apparent viscosity than the end of the first plot; this argued against ‘one way’ hypotheses such as stress-induced depolymerisation or dilution, while any sample ejection or detachment from the cone circumference must have been accompanied by effective recovery mechanisms.

Shear stress results from the initial steady shear measurement are also compared with data from a series of shear rate jumps between $\dot{\gamma} = 0.0005$ and 1.0 s^{-1} , in Fig. 7. Again, although the subsequent measurements were slightly lower than the initial results, all the data at $\dot{\gamma} = 1 \text{ s}^{-1}$ showed similar trends (Fig. 7a).

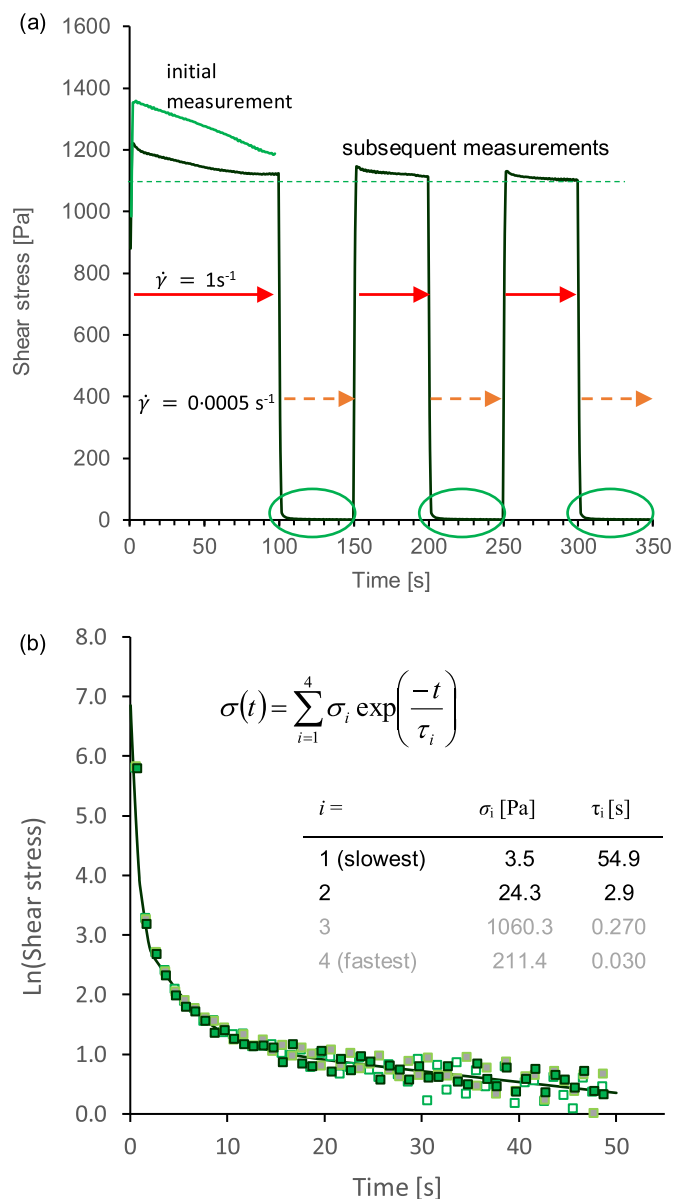


Fig. 7. Variations in shear stress during shear measurements. (a) Initial measurement over 100 s at $\dot{\gamma} = 1 \text{ s}^{-1}$ compared with subsequent measurements at 1 and 0.0005 s^{-1} ; the dashed line indicates the shear stress at the end of the final period at 1 s^{-1} . (b) Stress decay over time, following steps down from $\dot{\gamma} = 1$ to 0.0005 s^{-1} (measurement periods ringed in a); the different coloured symbols represent data from different experimental stages; the continuous line represents the multiple exponential decay model described by the equation with the fitting parameters shown (greyed data from oscillatory measurements).

Examples of stress relaxation results following the abrupt decreases in shear rate are presented in Fig. 7b. (The measurement periods are ringed in Fig. 7a.) Although measurements under static conditions were not possible with the present apparatus, reproducible results were obtained under ‘quasi-static’ conditions, at $\dot{\gamma} = 0.0005 \text{ s}^{-1}$. Following each step down to low shear rate, the stress appeared to decrease in a highly consistent manner. The largest part of the stress (over 95%) relaxed within 2 s; however, a small but significant fraction persisted until the end of each measurement period (50 s).

From a theoretical perspective, linear viscoelasticity is usually described using the Maxwell model, in terms of a conceptual system of a spring and dashpot in series [72–76]. In this mechanical analogy, an instantaneously applied step strain is initially accommodated by the spring stretching and an associated stress (σ) that decays exponentially as the dashpot responds:

$$\sigma(t) = \sigma_0 \cdot \exp\left(\frac{-t}{\tau}\right) \quad (3a)$$

where the characteristic time constant (τ) is given by the ratio of the viscosity to the shear modulus:

$$\tau = \frac{\eta}{G} \quad (3b)$$

While this simple conceptual model can reproduce the main features of polymer rheology, real systems generally exhibit multiple relaxation modes that may be described using a number of Maxwell models in parallel:

$$\sigma(t) = \sum_{i=1}^n \sigma_i \exp\left(\frac{-t}{\tau_i}\right) \quad (3c)$$

where σ_i and τ_i are the stress contribution and relaxation time of the i th component.

A model of this form with at least three terms was found to fit the data shown in Fig. 7b well. The parameters for the two slower modes were obtained by fitting the stress relaxation data, using the Solver tool in Excel, which gave relaxation times of 2.9 and 54.9 s. Comparable values ($3.4 \pm 0.5 \text{ s}$ and $66 \pm 22 \text{ s}$) were also obtained from similar measurements on other specimens.

This brief investigation suggested that the flow behaviour of silk protein solutions included contributions from relatively slow relaxation processes, which could affect apparent viscosity measurements for a considerable time (over 100 s). These relatively slow relaxation modes were probably associated with deformation of the average coil geometry in response to sudden changes (increases or decreases) in shear rates. Hence, it appears that most of the variations in apparent viscosity during individual experiments were probably caused by stress overshoot, due to these relatively slow relaxation modes, although minor contributions due to other effects cannot be completely ruled out. This will be explored in more detail during subsequent work.

It was not possible to extract the terms in Equation (3c) corresponding to the fastest stress relaxation modes (occurring within 2 s) directly from the stress relaxation measurements. Nevertheless, good agreement with the experimental data was achieved using parameters calculated from oscillatory measurements, as described in the next section.

3.3. Oscillatory measurements

Results from duplicate oscillatory sweeps at 25 °C, for a typical specimen of native silk feedstock are shown in Fig. 8. Note: this was the same specimen as used in the previously described stress

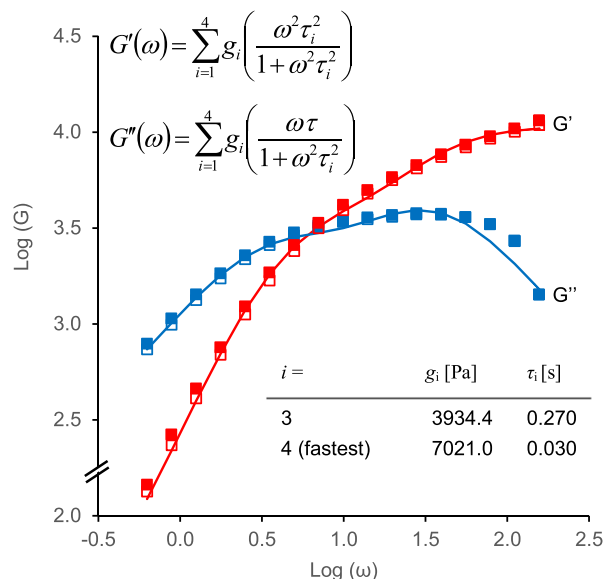


Fig. 8. Plots of elastic and viscous moduli vs. angular frequency, for native silk protein solution at 25 °C; the filled and open symbols represent duplicate measurements on the same specimen, before and after the stress relaxation measurements shown in Fig. 7. The continuous lines represent the best fits to G' and G'' data using the binary model described by the equations, using the parameters shown.

relaxation experiments, with the second oscillatory sweep performed after the stress relaxation measurements (*i.e.* approximately 6 min after the first oscillatory sweep). Only very small decreases in modulus values were observed from the first to the second oscillatory sweep; the experimental uncertainty over the timescales used for these experiments corresponded to less than $\pm 6\%$ of the values obtained.

In general, the plots of elastic and viscous moduli against angular frequency (ω) were characterised by two distinct regions: the elastic modulus dominated at higher frequencies ($G' > G''$), indicating that the applied oscillations were faster than the dominant molecular relaxation process; by contrast, the viscous modulus dominated at lower frequency ($G' < G''$), where the applied oscillations were slower than the dominant molecular relaxation. This behaviour has been reported previously for native silk protein solutions [76,80–85] and is typical of a polymer melt or concentrated solution, where entanglements constrain the rates of molecular relaxations in response to the applied oscillating strain.

The precise values of modulus (G_X) and angular frequency (ω_X) at the cross-over were obtained by interpolation. As the cross-over frequency may be regarded as the demarcation between solid-like and liquid-like behaviour, it provides an indication of the overall relaxation rate of the specimen. The values of G_X and ω_X also provide convenient means of comparison with previously published oscillatory measurements.

Generally, examination of data from repeated oscillatory sweeps revealed uncertainties of less than $\pm 6\%$ in the values obtained for G_X and ω_X . The distributions of results from 122 specimens are presented in Fig. 9. Values of G_X (in Fig. 9a) appeared to be roughly normally distributed, with mean 3338 Pa and standard deviation 666 Pa; ω_X (Fig. 9b) appeared to be significantly skewed, with a mode around 4.0 rad s^{-1} , a mean of 5.6 rad s^{-1} , a standard deviation of 2.5 rad s^{-1} and a considerably extended tail towards higher values. The ranges of results were considerably larger than the expected experimental uncertainties, indicating significant differences between the specimens analysed. Again, however, no obvious correlations could be found between these results and the physical conditions or storage times of the silkworms.

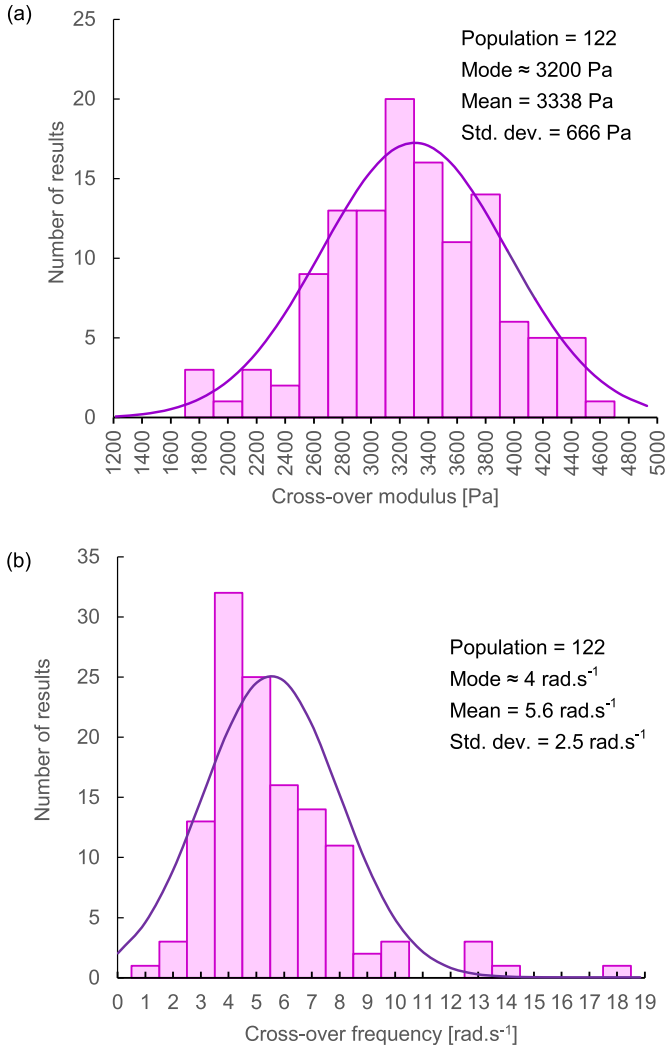


Fig. 9. Histograms showing the distributions of cross-over results for native silk protein solution specimens at 25 °C, based on the population size shown: (a) modulus, (b) angular frequency. The continuous lines represent the normal distributions approximating the results obtained, with the means and standard deviations shown.

These distributions of results appeared to be consistent with most of the previously reported work. The mean values of G_X and ω_X were similar to those reported by Terry *et al.* [65] and Holland *et al.* [82,84,85], slightly lower than those reported by Boulet-Audet *et al.* [81] but somewhat higher than those reported by Jin *et al.* [80]. By contrast, the results reported by Ochi *et al.* [77] did not show a cross-over, with the elastic modulus larger than the viscous modulus over the entire frequency range, suggesting that those specimens had gelled.

3.4. Determining modulus and relaxation times

For oscillatory measurements of viscoelasticity using a sinusoidal strain, the simple Maxwell model leads to the following well-known expressions:

$$G'(\omega) = G_N \left(\frac{\omega^2 \tau^2}{1 + \omega^2 \tau^2} \right) \quad (4a)$$

$$G''(\omega) = G_N \left(\frac{\omega \tau}{1 + \omega^2 \tau^2} \right) \quad (4b)$$

G_N represents the pure elastic modulus of the network of polymer chains, which corresponds to the 'plateau modulus' of G' measured at very high frequency. Although this simplistic model can qualitatively describe viscoelastic behaviour, real polymer systems generally involve multiple relaxation processes, corresponding to multiple 'Maxwell units' in parallel [72–75]. This leads to the following general expressions for the elastic and viscous moduli:

$$G'(\omega) = \sum_{i=1}^{\infty} p_i G_i \left(\frac{\omega^2 \tau_i^2}{1 + \omega^2 \tau_i^2} \right) \quad (5a)$$

$$G''(\omega) = \sum_{i=1}^{\infty} p_i G_i \left(\frac{\omega \tau_i}{1 + \omega^2 \tau_i^2} \right) \quad (5b)$$

where p_i is a weighting term that describes the relative abundance and G_i represents the modulus contribution of the i th mode.

In the present work, it was found that both the elastic and viscous moduli could be described reasonably well by binary expressions:

$$G'(\omega) = g_1 \left(\frac{\omega^2 \tau_1^2}{1 + \omega^2 \tau_1^2} \right) + g_2 \left(\frac{\omega^2 \tau_2^2}{1 + \omega^2 \tau_2^2} \right) \quad (6a)$$

$$G''(\omega) = g_1 \left(\frac{\omega \tau_1}{1 + \omega^2 \tau_1^2} \right) + g_2 \left(\frac{\omega \tau_2}{1 + \omega^2 \tau_2^2} \right) \quad (6b)$$

where g_i combines the modulus term and the weighting (*i.e.* $g_i = p_i G_i$). This binary model is compared with typical data from a specimen of native silk protein solution in Fig. 8. The model, represented by the continuous lines, provided a good fit to the G' data below $\log(\omega) = 1.6$ (corresponding to $\omega = 40 \text{ rad s}^{-1}$), although it deviated at higher frequencies. It also appeared to provide a good fit to the G' data across the majority of the range measured, with small undershoots at the lowest and highest frequencies. Note: the parameters listed in Fig. 8 are quoted for $i = 3$ and 4; as this was the same specimen as used for the stress relaxation measurements (Fig. 7), the parameters with $i = 1$ and 2 correspond to the slowest modes evaluated in that experiment.

Closer fits to experimental data achieved by including more (*i.e.* three or four) terms in the model. In particular, where it was available, a slightly better fit to the low frequency data was achieved by incorporating terms representing the slower modes evaluated from stress relaxation under quasi-static conditions. Following abrupt decreases in shear rate from $\dot{\gamma} = 1$ to 0.0005 s^{-1} , the modulus contributions for the slowest modes were calculated using:

$$g_i = \frac{\sigma_i}{\dot{\gamma} \tau_i} \quad (7)$$

where the shear rate corresponded to the faster flow ($\dot{\gamma} = 1 \text{ s}^{-1}$) just prior to the relaxation measurements. This was only available in a relatively few experiments, however. In other cases, attempts to evaluate the slower relaxation modes from the oscillatory data alone were unreliable. Models for G' and G'' incorporating three or more terms were prone to poor convergence, such that multiple attempted fits to the same data yielded variable values for the fitting parameters. Hence, the additional complexity was not justified for the experiments performed in this work.

The distributions of relaxation time constants revealed by analysing the oscillatory data from 115 experiments using the binary model are summarised in Fig. 10. Generally, the larger contribution

to the model (i.e. $g_i = 7145 \pm 1721$ Pa, mean \pm standard deviation) corresponded to the shorter relaxation time ($\tau_i = 55 \pm 16$ ms), while a smaller contribution ($g_i = 3701 \pm 1744$ Pa) corresponded to a longer relaxation time ($\tau_i = 442 \pm 122$ ms). Moreover, the distribution of the fastest relaxation times appeared to be bi-modal, with the main peak around $\tau = 60$ ms and a subsidiary peak around $\tau = 30$ ms. Again the expected uncertainties in measuring these data and fitting the model were less than $\pm 6\%$ of the values obtained for each parameter. Hence, these results also indicated significant variability between the specimens analysed.

In addition, to the relatively short relaxation modes revealed by oscillatory measurements, as previously described, two longer modes with τ_i around 3.4 and 66 s were obtained by fitting stress relaxation data, as in Fig. 7.

The different time constants may be ascribed to different relaxation mechanisms operating within the silk protein feedstock, with the slower modes involving longer range or concerted molecular motion [72–76,99]. Hence, it seems likely that the fastest relaxation ($\tau \approx 55$ ms) may correspond to changes in short-range turns and loops of a polymer chain within its reptation tube;

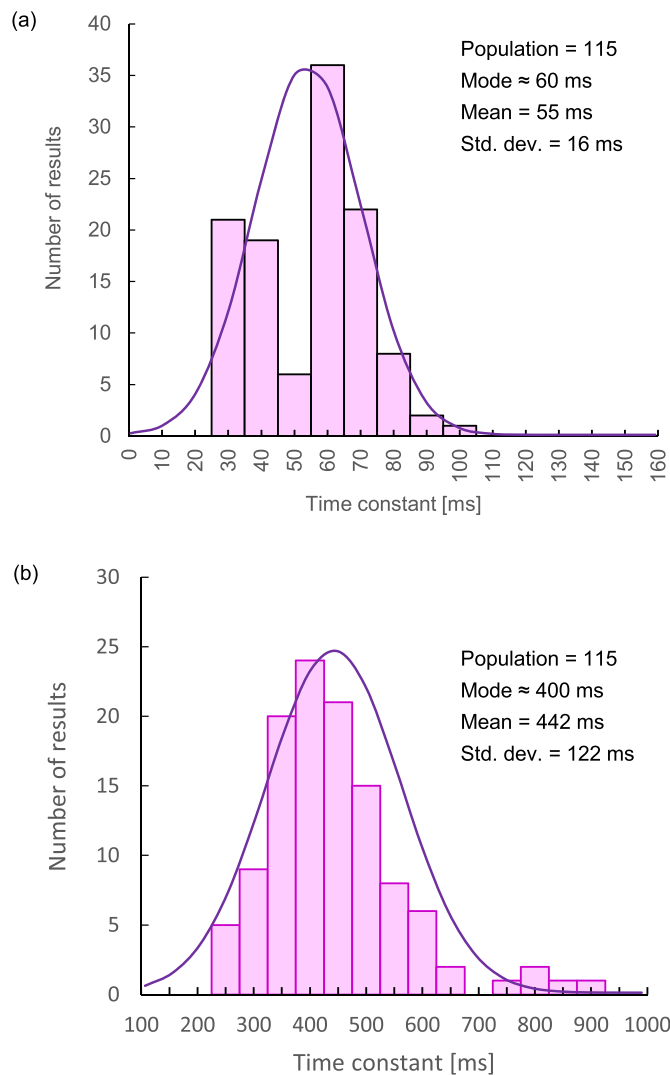


Fig. 10. Histograms showing the distributions of relaxation time constants revealed by analysing oscillatory data at 25 °C using the binary Maxwell model (Equation (6)), based on the population size shown: (a) for the faster relaxation process; (b) for the slower relaxation process. The continuous lines represent normal distributions approximating the results obtained, with the means and standard deviations shown.

these can relax or return to equilibrium by local motion of a few amino acid units, without affecting the tube contour. Other modes ($\tau \approx 442$ ms or 3.4 s) may correspond to retraction of polymer coils along their reptation tubes or changes in the overall tube contours. Following this hypothesis, the longest timescale ($\tau \approx 66$ s) suggests considerable concerted motion of neighbouring chains, involving whole protein molecules or even groups of molecules. These present suggestions are only conjectural, however, and considerable further work would be required to fully identify the processes involved.

3.5. Correlation between shear and oscillatory measurements

As a further check on the reliability of the experimental data, the shear viscosity measured at $\dot{\gamma} = 1 \text{ s}^{-1}$ was compared with estimates of the zero shear viscosity (η_0) based on oscillatory data. According to the Maxwell model [72–75], η_0 is expected to be related to the modulus contributions and relaxation time constants by:

$$\eta_0 = \sum_{i=1}^{\infty} g_i \tau_i \quad (8a)$$

As the oscillatory data was fitted well using a binary model (Equation (7)), it should be possible to estimate η_0 from the corresponding values of g_i and τ_i :

$$\eta_0 = g_1 \tau_1 + g_2 \tau_2 \quad (8b)$$

As shown in Fig. 11, the calculated values of η_0 correlated very well with the measured values of η_1 (correlation coefficient, $R^2 = 0.96$). This demonstrates the good accuracy of both the shear and oscillatory measurements, as random errors in either would decrease the correlation. Hence, the ranges of results observed for shear viscosity (Figs. 4–6) and viscoelasticity (Figs. 9 and 10) appear to reflect real variations within the specimens used. It is uncertain whether these variations were inherent in the native silk protein feedstocks within the silkworms or as a result of some poorly controlled (and presently unidentified) aspect of the sample

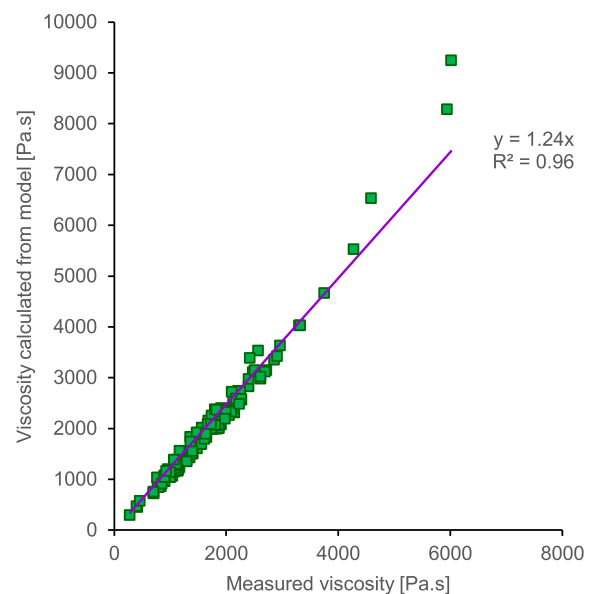


Fig. 11. Zero shear rate viscosity calculated by Equation (8b), using parameters from the binary Maxwell model (Equation (6)) against the shear viscosity measured at $\dot{\gamma} = 1 \text{ s}^{-1}$. The continuous line represents the best fit constrained to pass through the origin.

preparation or experimental methods. Inherent natural variation in the silk feedstock seems more likely, however, in view of the consistent procedures used to extract and analyse these specimens.

The 'best fit' straight line was constrained to pass through the origin (0,0), consistent with expectations. The resulting slope of 1.24 suggested that η_0 was slightly higher than η_1 , which may be explained by a small amount of shear thinning that was expected at the shear rate ($\dot{\gamma} = 1 \text{ s}^{-1}$) used [85]. Moreover, the slight upward curvature may be ascribed to slightly more shear thinning for the higher viscosity specimens, consistent with their slower relaxation rates.

3.6. Calculating molecular weight between entanglements

For measurements at sufficiently high frequency, entanglements between polymer chains have insufficient time to relax and behave as permanent cross-links. Under these conditions, as a rough approximation, the polymer chains in the silk protein solutions were expected to behave as a network of entropic springs. Hence, G_N was expected to depend on the number of contributing segments per unit volume (*i.e.* the chain segment density, ρ_c):

$$G_N = \rho_c k_B T \quad (9a)$$

where k_B is the Boltzmann constant and T is temperature. This leads to a simple estimation for the average molecular weight between entanglements (M_e):

$$M_e \approx \frac{\rho_c N_A k_B T}{G_N} \quad (9b)$$

$$= \frac{\rho c R T}{G_N} \quad (9c)$$

where R is the gas constant. The bulk density (ρ) of the native fibroin solution was estimated from the measured solids concentration, based on the assumption of conserved volume mixing of silk protein (density *ca.* 1300 kg m^{-3} [16,100,101]) and water.

It was not possible to observe the plateau modulus directly from the values of G' , which appeared to continue increasing beyond the highest frequency measurement used. Instead, G_N was estimated from the modulus contributions obtained by fitting the binary Maxwell model to the experimental data. At sufficiently high frequencies, $\omega\tau_i \gg 1$ and (from Equation (6a)):

$$G_N \approx g_1 + g_2 \quad (10)$$

As shown in Fig. 12b, the resulting values of M_e appeared to be normally distributed, with a mean of 66 kDa and standard deviation of 18 kDa.

It may be noted that similar or slightly (up to *ca.* 5%) higher estimates of M_e were also obtained by using the value of G' at the highest measured frequency as an approximation for G_N . This method was generally considered less reliable, however, since it depended on the accuracy of a single measurement.

These estimates of M_e were significantly smaller than the molecular weight of a heavy fibroin chain and corresponded to roughly one sixth of the fibH-fibL dimer. In other words, these results suggested around 6 to 7 entanglements per chain, which may seem surprisingly few for a reasonably concentrated solution (*i.e.* *ca.* 25% w/w) of a high molecular weight polymer (*i.e.* *ca.* 400 kDa for the fibH-fibL dimer). A potential explanation may be that the protein reduces its scope for entanglements by maintaining a rather dense coil configuration, such as the 'string of beads' model proposed by Vollrath and Porter [50]; this could arise due to the prevailing

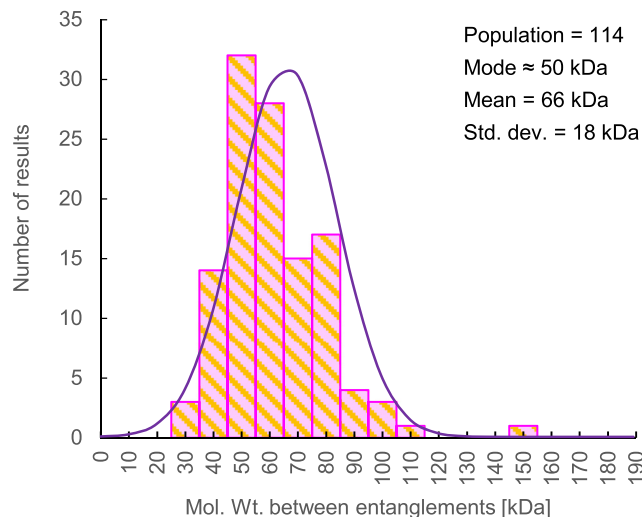


Fig. 12. Histograms showing the distribution of the molecular weight between entanglements, based on the population size shown, calculated using Equation (9) and the plateau modulus estimated from the binary Maxwell model (Equations (6) and (10)). The continuous lines represent the normal distributions approximating the results obtained, with the mean and standard deviation shown.

hydrophobicity of the repetitive amino acid sequences, as suggested by Sehnal and Žurovec [20].

These estimates were also significantly smaller than the value reported by Moriya et al. [78], based on a similar analysis of comparable data. It appears, however, that their estimate contained an error; by omitting the concentration term, in effect, they obtained the molecular weight of solution (*i.e.* polymer chain plus associated water) between entanglements. Allowing for concentration (*ca.* 25%), their result would be around 85 kDa, which is comparable to our estimates.

4. Discussion and conclusions

The results from the present work are summarised in Table 1. These suggest that, provided they are handled appropriately, native silk feedstocks are well-behaved viscoelastic systems, with characteristics similar to other conventional polymer solutions. Our results were generally consistent with previously published data and constitute the largest dataset obtained to date, providing representative, 'gold standard' data for *B. mori*. Hence, this will form a sound basis for further investigations into the polymer science underlying silk fibre production, including parameterisation of flow simulations and assessing the quality of biomimetic feedstocks.

Nevertheless, the results exhibited considerable variability, which cannot readily be explained by experimental uncertainties in the measurements made. This was manifest in the solids content, shear viscosity and viscoelastic properties (*i.e.* cross-over modulus and frequency), as well as the derived properties (*i.e.* relaxation time constants and molecular weight between entanglements).

It is known that the native silk feedstocks are exquisitely sensitive to flow [54,65] and may be induced to gel by excessively vigorous handling. This did not appear to be a contributory factor in the current work, however, which was built on a decade of in-house experience handling these materials and carefully refined experimental techniques. On the other hand, a certain amount of natural variability might be expected in the silk feedstocks, as a result of differences between the individual silkworms – even though the specimens for analysis were all obtained from *B. mori* larvae at a similar developmental stage. This aspect of inherent natural variability has been rather overlooked in previous work.

Table 1
Summary of rheological results for native silk protein solution specimens (from the MP gland division of 5th instar *B. mori* silkworms at the start of cocoon construction).

Measurement method	Physical property	Mean	Standard deviation (population size)
Gravimetry	Protein concentration [% w/w]	24.0	2.5 (N = 124)
Shear viscosity	Viscosity at $\dot{\gamma} = 1 \text{ s}^{-1}$ [Pa s]	1722	935 (N = 125)
Stress relaxation	Time constant, τ_1 [s]	66	22 (N = 5)
	Modulus contribution, g_1 [Pa]	0.11	0.08 (N = 5)
Stress relaxation	Time constant, τ_2 [s]	3.4	0.5 (N = 5)
	Modulus contribution, g_2 [Pa]	9.3	4.3 (N = 5)
Oscillatory sweep	Time constant, τ_3 [s]	0.442	0.016 (N = 115)
	Modulus contribution, g_3 [Pa]	3701	1744 (N = 115)
Oscillatory sweep	Time constant, τ_4 [s]	0.055	0.016 (N = 115)
	Modulus contribution, g_4 [Pa]	7145	1721 (N = 115)
Oscillatory sweep	Cross-over modulus [Pa]	3338	666 (N = 122)
	Cross-over frequency [rad s^{-1}]	5.6	2.5 (N = 122)
Mol. wt. between entanglements [kDa] from binary model		66	18 (N = 118)

In spite of the evident variability in the gland contents, however, it appeared that all the silkworms used were capable of spinning normal silk to form normal cocoons. Indeed, most specimens were sacrificed during the early stages of pupation, having laid down anchor lines and started on cocoon construction. It would be interesting to explore whether the rheological variations observed in this work could affect the silkworm's ability to spin or the physical properties of the resultant silk.

Although the present work demonstrated considerable variability in shear viscosity and viscoelasticity, along with the derived estimates of average molecular weight between entanglements, it did not explore the causes in any detail. Clearly, this must be a key objective for further work. In particular, specific methods to investigate the molecular weight distributions (e.g. gel permeation chromatography, gel electrophoresis or ultracentrifugation) and solution structure (e.g. small-angle X-ray and neutron scattering) could be very informative and are the subject of current investigations, which will be reported subsequently.

Acknowledgements

This work was funded by the EPSRC, project reference EP/K005693/1. We are grateful to R.T. Ramsdale-Capper (University of Sheffield) for constructing the environmental cover for the rheometer. We would also like to thank Prof. T.C.B. McLeish (Durham University) and Dr. A. Terry (ISIS, RAL) for helpful discussions during the preparation of this manuscript.

References

- Craig CL. Evolution of arthropod silks. *Annu Rev Entomol* 1997;42:231–67.
- Brunetta L, Craig CL. Spider silk. New Haven: Yale University Press; 2010.
- Eisoldt L, Smith A, Scheibel T. Decoding the secrets of spider silk. *Mats Today*. 2011;14:80–6.
- Bond JE, Garrison NL, Hamilton CA, Godwin RL, Agnarsson I. Phylogenomics resolves a spider backbone phylogeny and rejects a prevailing paradigm for orb web evolution. *Curr Biol* 2014;24:1765–71.
- Sehnal F, Sutherland T. Silks produced by insect labial glands. *Prion* 2008;2:145–53.
- Sutherland TD, Peng YY, Trueman HE, Weisman S, Okada S, Walker AA, et al. A new class of animal collagen masquerading as an insect silk. *Sci Rep* 2013;3:2864. <http://dx.doi.org/10.1038/srep02864>.
- Sutherland T, Weisman S, Walker AA, Mudie ST. The coiled coil silk of bees, ants and hornets. *Biopolymers* 2011;97:446–54.
- Sutherland TD, Young JH, Weisman S, Hayashi CH, Merritt DJ. Insect silk: one name, many materials. *Annu Rev Entomol* 2010;55:171–88.
- Walker AA, Church JS, Woodhead AL, Sutherland TD. Silverfish silk is formed by entanglement of randomly coiled protein chains. *Insect Biochem. Mol Biol* 2013;43:572–9.
- Collin MA, Edgerley JS, Hayashi CY. Comparison of fibroin cDNAs from web-spinning insects: insight into silk formation and function. *Zoology* 2011;114:239–46.
- Lewis JGE. The biology of centipedes. Cambridge University Press; 1981. <http://dx.doi.org/10.1017/CBO9780511565649>.
- Dong Z, Zhao P, Wang C, Zhang Y, Chen J, Wang X, et al. Comparative proteomics reveal diverse functions and dynamic changes of *Bombyx mori* silk proteins spun from different development stages. *J Proteome Res* 2013;12:5213–22.
- Hooper L. Silk: its production and manufacture. London: Sir Isaac Pitman & Sons Ltd; 1911.
- Datta RK, Nanavaty N. Global silk industry: a complete sourcebook. Boca Raton, USA: Universal Publishers; 2005.
- Popescu A. Trends in world silk cocoons and silk production and trade, 2007–2010. *Anim Sci Biotech* 2013;46:418–23.
- Babu KM. Silk: processing, properties and applications. Cambridge: Woodhead Publishing Ltd; 2013.
- Craig CL, Riekel C. Comparative architecture of silks, fibrous proteins and their encoding genes in insects and spiders. *Comp Biochem Physiol B* 2002;133:493–507.
- Fu C, Shao Z, Vollrath F. Animal silks: their structures, properties and artificial production. *Chem Commun* 2009:6515–29.
- Gosline JM, Guerette PA, Ortlepp CS, Savage KN. The mechanical design of spider silks: from fibroin sequence to mechanical function. *J Exp Biol* 1999;202:3295–303.
- Sehnal F, Zurovec M. Construction of silk fiber core in lepidoptera. *Bio-macromolecules* 2004;5:666–74.
- Xu G, Gong L, Yang Z, Liu XY. What makes spider silk fibres so strong? from molecular-crystallite network to hierarchical network structures. *Soft Mater*. 2014;10:2116–23.
- Seydel T, Kölln K, Krasnov I, Diddens I, Hauptmann N, Helms G, et al. Silk-worm silk under tensile strain investigated by synchrotron X-ray diffraction and neutron spectroscopy. *Macromolecules* 2007;40:1035–42.
- Riekel C, Vollrath F. Spider silk fibre extrusion: combined wide- and small-angle X-ray microdiffraction experiments. *Int J Biol Macromol* 2001;29:203–10.
- Lotz B, Keith HD. Crystal structure of poly(L-Ala-Gly)II: a model for silk I. *J Mol Biol* 1971;61:201–15.
- Fraser RDB, MacRae, Stewart FHC. Poly-L-alanyl-glycyl-L-alanyl-glycyl-L-seryl-glycine: a model for the crystalline regions of silk fibroin. *J Mol Biol* 1966;19:580–2.
- Eisoldt L, Thamm C, Scheibel T. The role of terminal domains during storage and assembly of spider silk proteins. *Biopolymers* 2012;97:355–61.
- He Y-X, Zhang N-N, Li W-F, Jia N, Chen B-Y, Zhou K, et al. N-terminal domain of *Bombyx mori* fibroin mediates the assembly of silk in response to pH decrease. *J Mol Biol* 2012;418:197–207.
- Hagn F, Thamm C, Scheibel T, Kessler H. pH-dependent dimerization and salt-dependent stabilization of the N-terminal domain of spider dragline silk – implications for fiber formation. *Angew Chem Int Ed* 2011;50:310–3.
- Gaines WA, Sehorn MG, Marcotte WR. Spidroin N-terminal domain promotes a pH-dependent association of silk proteins during self-assembly. *J Biol Chem* 2010;285:40745–53.
- Zhou P, Xie X, Knight DP, Zong X-H, Deng F, Yao W-H. Effects of pH and calcium ions on the conformational transitions in silk fibroin using 2D Raman correlation spectroscopy and ^{13}C solid-state NMR. *Biochemistry* 2004;43:11302–11.
- Knight DP, Vollrath F. Changes in element composition along the spinning duct in a *Nephila* spider. *Naturwissenschaften* 2001;88:179–82.
- Zhou C-Z, Confalonieri F, Medina N, Zivanovic Y, Esnault C, Yang T, et al. Fine organization of *Bombyx mori* fibroin heavy chain gene. *Nucl Acids Resch* 2000;28:2413–9.
- Manning RF, Gage LP. Internal structure of the silk fibroin gene of *Bombyx mori*. II Remarkable polymorphism of the organization of crystalline and amorphous coding sequences. *J Biol Chem* 1980;255:9451–7.
- Gamo T, Inokuchi T, Laufer H. Polypeptides of fibroin and sericin secreted from the different sections of the silk gland in *Bombyx mori*. *Insect Biochem.* 1977;7:285–95.
- Gene and corresponding amino-acid sequences for silk proteins of *B. mori* and several wild species are available at GenBank. <http://www.ncbi.nlm.nih.gov/genbank/>.

- [36] Tanaka K, Kajiyama N, Ishikura K, Waga S, Kikuchi A, Ohtomo K, et al. Determination of the site of disulphide linkage between heavy and light chains of silk fibroin produced by *Bombyx mori*. *Biochim Biophys Acta* 1999;1432:92–103.
- [37] Tanaka K, Mori K, Mizuno S. Immunological identification of the major disulphide-linked light component of silk fibroin. *J Biochem* 1993;114:1–4.
- [38] Shimura K, Kikuchi A, Katagata Y, Ohtomo A. The occurrence of small component proteins in the cocoon fibroin of *Bombyx mori*. *J Seric Sci Jpn* 1982;51:20–6.
- [39] Mori K, Tanaka K, Kikuchi Y, Waga M, Waga S, Mizuno S. Production of a chimeric fibroin light-chain polypeptide in a fibroin secretion-deficient naked pupa mutant of the silkworm *Bombyx mori*. *J Mol Biol* 1995;251:217–28.
- [40] Takei F, Kikuchi Y, Kikuchi A, Mizuno S, Shimura K. Further evidence for importance of the subunit combination of silk fibroin in its efficient secretion from the posterior silk gland cells. *J Cell Biol* 1987;105:175–80.
- [41] Takei F, Oyama F, Kimura K-I, Hyodo A, Mizuno S, Shimura K. Reduced level of secretion and absence of subunit combination for the fibroin synthesised by a mutant silkworm, Nd(2). *J Cell Biol* 1984;99:2005–10.
- [42] Chevillard M, Couble P, Prudhomme J-C. Complete nucleotide sequence of the gene encoding the *Bombyx mori* silk protein P25 and predicted amino acid sequence of the protein. *Nucleic Acids Res* 1986;14:6341–2.
- [43] Chevillard M, Deleage G, Couble P. Amino acid sequence and putative conformational characteristics of the 25kD silk protein of *Bombyx mori*. *Sericologia* 1986;26:435–49.
- [44] Couble P, Chevillard M, Moine A, Ravel-Chapuis P, Prudhomme J-C. Structural organization of the P25 gene of *Bombyx mori* and comparative analysis of the 5' flanking DNA with that of the fibroin gene. *Nucleic Acids Res* 1985;13:1801–14.
- [45] Couble P, Moine A, Garel A, Prudhomme J-C. Developmental variations of a non-fibroin mRNA of *Bombyx mori* silk gland, encoding for a low-molecular-weight protein. *Dev Biol* 1983;97:398–407.
- [46] Inoue S, Tanaka K, Arisaka F, Kimura S, Ohtomo K, Mizuno S. Silk fibroin of *Bombyx mori* is secreted, assembling a high molecular mass elementary unit consisting of H-chain, L-chain and P25, with a 6:6:1 molar ratio. *J Biol Chem* 2000;275:40517–28.
- [47] Tanaka K, Mizuno S. Homologues of fibroin L-chain and P25 of *Bombyx mori* are present in *dendrolimus spectabilis* and *papilio xuthus* but not detectable in *Antheraea yamamai*. *Insect Biochem Mol Biol* 2001;31:665–77.
- [48] Hou Y, Xia Q, Zhao P, Zou H, Guan J, Gong J, et al. Studies on middle and posterior silk glands of silkworm (*Bombyx mori*) using two-dimensional electrophoresis and mass spectrometry. *Insect Biochem Mol Biol* 2007;37:486–96.
- [49] Porter D, Vollrath F. Silk as a biomimetic ideal for structural polymers. *Adv Mats* 2009;21:487–92.
- [50] Vollrath F, Porter D. Silk as archetypal protein elastomer. *Soft Matter* 2006;2:337–85.
- [51] Vollrath F, Porter D, Holland C. The science of silks. *MRS Bull* 2013;38:73–80.
- [52] Shao Z, Vollrath F. Surprising strength of silkworm silk. *Nature* 2002;418:741.
- [53] Vollrath F, Knight DP. Liquid crystalline spinning of spider silk. *Nature* 2001;410:541–8.
- [54] Holland C, O'Neil K, Vollrath F, Dicko C. Distinct structural and optical regimes in natural silk spinning. *Biopolymers* 2012;97:368–73.
- [55] Downes AM, Sharry LF. Measurement of wool growth and its response to nutritional changes. *Aust J Biol Sci* 1971;24:117–30.
- [56] Chen X, Shao Z, Vollrath F. The spinning processes for spider silk. *Soft Matter* 2006;2:448–51.
- [57] Porter D, Guan J, Vollrath F. Spider silk: super material or thin fibre? *Adv Mats* 2013;25:1275–9.
- [58] Mortimer B, Holland C, Vollrath F. Forced reeling of *Bombyx mori* silk: separating behavior and processing conditions. *Biomacromolecules* 2013;14:3653–9.
- [59] Blamires SJ, Wu C-L, Blackledge TA, Tso I-M. Post-secretion processing influences spider silk performance. *J R Soc Interface* 2012;9:2479–87.
- [60] Blamires SJ, Wu C-L, Blackledge TA, Tso I-M. Environmentally induced post-spin property changes in spider silks: influences of web type, spidroin composition and ecology. *Biol J Linn Soc* 2012;106:580–8.
- [61] Belén-Perea G, Plaza GR, Guinea GV, Elices M, Velasco B, Pérez-Riguero J. The variability and interdependence of spider viscid line tensile properties. *J Exp Biol* 2013;216:4722–8.
- [62] Omenetto FG, Kaplan DL. New opportunities for an ancient material. *Science* 2010;329:528–31.
- [63] Iizuka E. Mechanism of fibre formation by the silkworm *Bombyx mori*. *Biorheology* 1966;3:141–52.
- [64] Holland C, Vollrath F, Ryan AJ, Mykhaylyk OO. Silk and synthetic polymers: reconciling 100 degrees of separation. *Adv Mater* 2012;24:105–9.
- [65] Terry AE, Knight DP, Porter D, Vollrath F. pH induced changes in the rheology of silk fibroin solution from the middle division of *Bombyx mori* silkworm. *Biomacromolecules* 2004;5:768–72.
- [66] Holland C, Urbach JS, Blair DL. Direct visualization of shear dependent silk fibrillogenesis. *Soft Matter* 2012;8:2590–4.
- [67] Leclerc J, Lefevre T, Gauthier M, Gagne SM, Auger M. Hydrodynamical properties of recombinant spider silk proteins: effects of pH, salts and shear, and implications for the spinning process. *Biopolymers* 2013;99:582–93.
- [68] Leclerc J, Lefevre T, Pottier F, Morency L-P, Lapointe-Verreault C, Gagné SM, et al. Structure and pH-induced alterations of recombinant and natural spider silk proteins in solution. *Biopolymers* 2011;97:337–46.
- [69] Dicko C, Kenney JM, Knight D, Vollrath F. Transition to a β -sheet-rich structure in spidroin in vitro: the effects of pH and cations. *Biochemistry* 2004;43:14080–7.
- [70] Gupta VB, Kothari VK, editors. *Manufactured fibre technology*. London: Chapman and Hall; 1997.
- [71] Moncrief RW. *Man-made fibres*. London: Newnes-Butterworths; 1975.
- [72] Goodwin JW, Hughes RW. *Rheology for chemists*. Cambridge: Royal Society of Chemistry; 2008.
- [73] Sunthar P. *Polymer rheology*. In: Deshpande AP, Krishnan JM, Kumar S, editors. *Rheology of complex fluids*. New York: Springer; 2010.
- [74] Ferry JD. *Viscoelastic properties of polymers*. 3rd ed. John Wiley & Sons Inc; 1980.
- [75] Watanabe H. Viscoelasticity and dynamics of entangled polymers. *Prog Poly Sci* 1999;24:1253–1403.
- [76] Vega JF, Rastogi S, Peters GWM, Meijer HEH. Rheology and reptation of linear polymers. Ultrahigh molecular weight chain dynamics in the melt. *J Rheol* 2004;48:663–78.
- [77] Ochi A, Hossain KS, Magoshi J, Nemoto N. Rheology and dynamic light scattering of silk fibroin solution extracted from the middle division of *Bombyx mori* silkworm. *Biomacromolecules* 2002;3:1187–96.
- [78] Moriya M, Ohgo K, Masubuchi Y, Asakura T. Flow analysis of aqueous solution of silk fibroin in the spinneret of *Bombyx mori* silkworm by combination of viscosity measurement and finite element method calculation. *Polymer* 2008;49:952–6.
- [79] Wang H, Mao N, Hu X, Shao H, Jin X. The properties of native silk fibroin (SF) solution/gel from *Bombyx mori* silkworms during the full fifth instar larval stage. *J Wuhan Univ Technol-Mater Sci Edn* 2011;26:262–8.
- [80] Jin Y, Hang Y, Juo J, Zhang Y, Shao H, Hu X. *In vitro* studies on the structure and properties of silk fibroin aqueous solutions in silkworm. *Int J Biol Macromol* 2013;62:162–6.
- [81] Boulet-Audet M, Terry AE, Vollrath F, Holland C. Silk protein aggregation kinetics revealed by Rheo-IR. *Acta Biomater* 2014;10:776–84.
- [82] Holland C, Porter D, Vollrath F. Comparing the rheology of mulberry and 'wild' silkworm spinning dopes. *Biopolymers* 2012;97:362–7.
- [83] Moriya M, Roschztzardt F, Nakahara Y, Saito H, Masabuchi Y, Asakura T. Rheological properties of native silk fibroins from domestic and wild silkworms, and flow analysis in each spinneret by a finite element method. *Biomacromolecules* 2009;10:929–35.
- [84] Holland C, Terry AE, Porter D, Vollrath F. Comparing the rheology of native spider and silkworm spinning dope. *Nat Mats* 2006;870–4.
- [85] Holland C, Terry AE, Porter D, Vollrath F. Natural and unnatural silks. *Polymer* 2007;48:3388–92.
- [86] Chen X, Knight DP, Vollrath F. Rheological characterization of *Nephila* spidroin solution. *Biomacromolecules* 2002;3:644–8.
- [87] Kojić N, Bico J, Clasen C, McKinley GH. *Ex vivo* rheology of spider silk. *J Exp Biol* 2006;209:4355–62.
- [88] Chen X, Knight DP, Shao Z, Vollrath F. Regenerated *Bombyx* silk solutions studied with rheometry and FTIR. *Polymer* 2001;42:9969–74.
- [89] Raghu A, Somashekar R, Sharath A. Microrheological studies of regenerated silk fibroin solution by video microscopy. *J Polym Sci B Polym Phys* 2007;45:2555–62.
- [90] Raghu A, Sharath A. Nanorheology of regenerated silk fibroin solution. *Bull Mater Sci* 2008;31:359–65.
- [91] Nagarkar S, Patil A, Lele A, Bhat S, Bellare J, Mashelkar RA. Some mechanistic insights into the gelation of regenerated silk fibroin sol. *Ind Eng Chem Res* 2009;48:8014–23.
- [92] Nisal A, Kallekalk A, Bellare J, Lele A. Rheology and microstructural studies of regenerated silk fibroin solutions. *Rheol Acta* 2013;52:833–40.
- [93] Lakkegowda Y, Ammannappa R, Ananthamurthy S. Investigations on rheological properties and gelation of tasar regenerated silk fibroin solution. *J Appl Polym Sci* 2013. <http://dx.doi.org/10.1002/APP.40104>.
- [94] Wang Q, Yang Y, Chen X, Shao Z. Investigation of rheological properties and conformation of silk fibroin in the solution of AmimCl. *Biomacromolecules* 2012;13:1875–81.
- [95] Siddiqui SA, Pandey AK, Dwivedi A, Jain S, Misra N. Comparative conformational, structural and vibrational study on the molecular structure of tyrosine and L-DOPA using density functional theory. *J Chem Pharm Res* 2010;2:835–50.
- [96] Barth A. The infrared absorption of amino acid side chains. *Prog Biophys Mol Biol* 2000;74:141–73.
- [97] Teramoto H, Miyazawa M. Molecular orientation behaviour of silk sericin film as revealed by ATR infrared spectroscopy. *Biomacromolecules* 2005;6:2049–57.
- [98] Zhou L, Terry AE, Huang Y-F, Shao Z-Z, Chen X. Metal element contents in silk gland and silk fiber of *Bombyx mori* silkworm. *Acta Chim Sin* 2005;15:1379–82.
- [99] Doi M, Edwards SF. *The theory of polymer dynamics*. Oxford: Clarendon Press; 1986.
- [100] Esmaili M, Fløystad JB, Diaz A, Høydaalsvik K, Guizar-Sicairos M, Andreassen JW, et al. Ptychographic X-ray tomography of silk fiber hydration. *Macromolecules* 2013;46:434–9.
- [101] Sen K, Babu KM. Studies on Indian silk. I. Macrocharacterization and analysis of amino acid composition. *J Appl Polym Sci* 2004;92:1080–97.